

# Design of ZnO:Al films with optimized surface texture for silicon thin-film solar cells

Michael Berginski<sup>\*a</sup>, Bernd Rech<sup>a</sup>, Jürgen Hüpkes<sup>a</sup>, Helmut Stiebig<sup>a</sup>, Matthias Wuttig<sup>b</sup>

<sup>a</sup>Institute of Photovoltaics (IPV), Forschungszentrum Jülich GmbH, 52425 Jülich, Germany;

<sup>b</sup>Institute of Physics (IA), RWTH Aachen University, 52056 Aachen, Germany

## ABSTRACT

This study addresses the design of radio frequency (rf) magnetron sputtered aluminum doped zinc oxide (ZnO:Al) front contacts for silicon thin-film solar cells. Optimized films comprise high conductivity and transparency, as well as a surface topography trapping the light within the photovoltaically active layers. We have investigated the influence of the doping level of the target as well as the substrate temperature during sputter deposition on the ZnO:Al properties. The aluminum content in the target influences the transmission in the near infrared (NIR), the conductivity as well as the film growth of the ZnO:Al layer. The latter affects the surface topography which develops during wet-chemical etching in diluted hydrochloric acid. Depending on aluminum content in the target and heater temperature three different regimes of etching behavior have been identified. We have applied the ZnO:Al films as front contacts in thin-film silicon solar cells to study their light trapping ability. While high transparency is a prerequisite, the light trapping has been improved using front contacts with a surface topography consisting of relatively uniformly dispersed craters. We have identified low amount of target doping and high substrate temperatures as sputter parameters enabling high cell currents. Short-circuit current densities of up to  $26.8 \text{ mA/cm}^2$  have been realized in  $\mu\text{-Si:H}$  single junction cell with absorber layer thickness of  $1.9 \mu\text{m}$ .

**Keywords:** thin-film solar cells, light trapping, zinc oxide, sputtering, microcrystalline silicon, aluminum doping level, transparent conductive oxide, TCO

## 1. INTRODUCTION

One promising thin-film solar cell approach employs cell concepts on cheap substrates (like float glass) with hydrogenated amorphous (a-Si:H) or microcrystalline silicon ( $\mu\text{-Si:H}$ ) as active layers. In case of silicon thin-film solar cells an efficient light trapping scheme is essential to enhance the intrinsically low absorbance of silicon especially in long wavelength range. Light trapping is achieved by combining textured transparent conductive oxide (TCO) films as front contacts with highly reflective back contacts. However, due to the multiple passes of scattered light within the solar cell device, parasitic light absorption in the photovoltaically non-active layers is increased as well.

In p-i-n configuration the cell is illuminated through TCO coated glass. The TCO has to meet counteracting properties: high conductivity to obtain low series resistance and low carrier concentration to avoid absorption losses in the red and near infrared (NIR) wavelength range. Note, that in the NIR the absorbance of a single pass through a  $1 \mu\text{m}$  thick layer of  $\mu\text{-Si:H}$  is lower than that of typical TCOs. Preceding work by Agashe et al. [1] studied the influence of the target doping concentration on the electrical and optical properties of sputter deposited ZnO:Al films. They found much lower parasitic absorptions using sputter targets with low amount of alumina.

Besides the transparency, a TCO with a suitable texture has to be developed which scatters the light very efficiently in order to elongate the effective path length within the active silicon layers. Thus, a special design of the TCO is necessary to fulfill all these requirements. For initially smooth sputter deposited ZnO:Al films a surface texture is realized by post-deposition wet-chemical etching. Kluth et al. [2] related the influence of pressure and substrate temperature during radio frequency sputter deposition of ZnO:Al to the post-etching surface topography in a modified Thornton model. They showed that, depending on sputter parameters, crater-like surface topography with typical lateral length scales of 1 to  $2 \mu\text{m}$  and depths of about 200 to 400 nm develops in a self-organized fashion.

In this work we study the role of the target aluminum concentration on the optimization of surface textured ZnO:Al films for the use in silicon thin-film solar cells. We briefly show optical and electrical properties confirming the results of Agashe et al. We focus on a reinterpretation of the modified Thornton model by Kluth et al. [2] in the way, that the

aluminum concentration in the target is introduced as new parameter to control the film properties. Not only sputter pressure and substrate temperature decide about the surface texture after etching, but also the aluminum concentration in the target and hence in the films. On the path on designing an optimized front TCO for thin-film solar cells, we study the influence of surface texture and NIR-transparency on the light trapping ability.

## 2. EXPERIMENT

ZnO:Al films have been prepared on Corning 1737 glass by rf magnetron sputtering from ceramic targets. The amount of doping has been varied using ZnO:Al<sub>2</sub>O<sub>3</sub> targets with 0.2, 0.5, 1 or 2 wt.% Al<sub>2</sub>O<sub>3</sub>. The concentration of Al<sub>2</sub>O<sub>3</sub> in the target is henceforth referred to as TAC. At constant deposition pressure of 0.3 Pa the substrate temperature has been varied in a range of 60 – 490 °C. Substrate temperatures were calibrated by a thermal sensor at constant heater temperatures. Film characterization was performed by four-point probe, room temperature Hall effect measurements and x-ray diffraction analysis. Optical transmittance and reflectance of smooth films were measured in air with a dual beam spectrometer. For textured ZnO:Al films CH<sub>2</sub>I<sub>2</sub> as index-matching fluid was applied to avoid systematic measurement errors due to light scattering of the rough films. After deposition, approximately 800 nm thick initially smooth films (root-mean-square (RMS) roughness about 15 nm) became surface-textured with typical RMS roughness of more than 100 nm by wet-chemical etching in diluted hydrochloric acid (0.5 % HCl). The surface topography and characteristic feature sizes were studied by scanning electron microscopy (SEM) and atomic force microscopy (AFM). The most effective way to characterize the light trapping ability of a specific TCO film is the application in solar cells. For this purpose, we have deposited μc-Si:H single junction solar cells using plasma enhanced chemical vapor deposition (PECVD) at 13.56 MHz excitation frequency in a 30x30 cm<sup>2</sup> reactor. Sputter deposited double layers of ZnO:Al (80 nm) and thermally evaporated silver (700 nm) served as back-reflector and rear side contact. Details of cell preparation are described elsewhere [3,4]. Solar cell characteristics have been measured using a sun simulator (Wacom-WXS-140S-Super) at standard test conditions (AM 1.5, 100 mW/cm<sup>2</sup> at 25 °C). The differential spectral response (DSR), at zero bias, of some solar cells has been measured and used to obtain the external quantum efficiency (QE). The short circuit current density, which corresponds with the maximal current density generated by the solar cell, is calculated employing the measured external quantum efficiency data and using the AM1.5 solar spectrum with an illumination density of 100 mW/cm<sup>2</sup> with the corresponding photon flux. Henceforth the short circuit current density calculated in this way is referred to as cell current.

## 3. RESULTS AND DISCUSSION

### 3.1 Optical and electrical ZnO:Al film properties

The TAC influences the amount of Al-doping and by this determines the number of free carriers in the ZnO:Al films [5]. This mainly affects the absorption of NIR light in the films [1,5] and shifts the fundamental absorption band edge (Burstein-Moss shift [6,7]). Fig.1 shows transmission and absorption spectra of ZnO:Al films sputtered at a fixed substrate temperature of 375 °C using 0.2%, 0.5% and 2.0% TAC. The absorption spectrum is calculated using spectrometer measurement data of transmission and reflection (not shown). Increasing the TAC raises the carrier density in the sputtered films (see inset in Fig.1 for carrier densities N in 10<sup>20</sup> cm<sup>-3</sup> measured in Hall experiments). Simultaneously the resistivities ρ (see inset, values are given in 10<sup>-3</sup> Ωcm) decrease. This leads to a shift of the fundamental absorption edge to smaller wavelengths (partially masked by the index matching fluid used) and at the same time to an increased parasitic free carrier absorption in the NIR spectral region. This absorption mechanism reduces the transmission significantly in the active range of the solar cells (up to about 1100 nm) for high doping levels. Films with higher carrier density show lower resistivity. A compromise has to be found between transmission and conductivity in order to prepare optimized ZnO:Al front contacts for solar cells. However, even though high transmission is a prerequisite, earlier work has shown that surface roughness, feature size and shape are key parameters for highly efficient light trapping [8,9]. Thus, we concentrate in the following section on the structural properties of the ZnO:Al films, which result in different etching behavior.

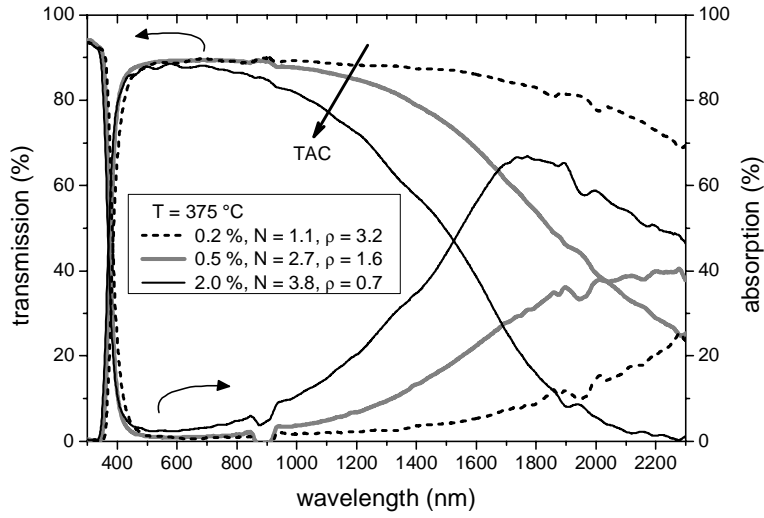


Figure 1: Transmission (left axis) and absorption (right axis) spectra of surface-textured front contacts sputtered at substrate temperature of 375 °C using ZnO:Al<sub>2</sub>O<sub>3</sub> targets with 0.2, 0.5 and 2.0 wt.% TAC. The absorption can only be considered for  $\lambda > 400$  nm, as CH<sub>2</sub>I<sub>2</sub> is strongly absorbing for smaller wavelengths. The discontinuity in the data around  $\lambda = 900$  nm is due to an artifact of the measurement system.

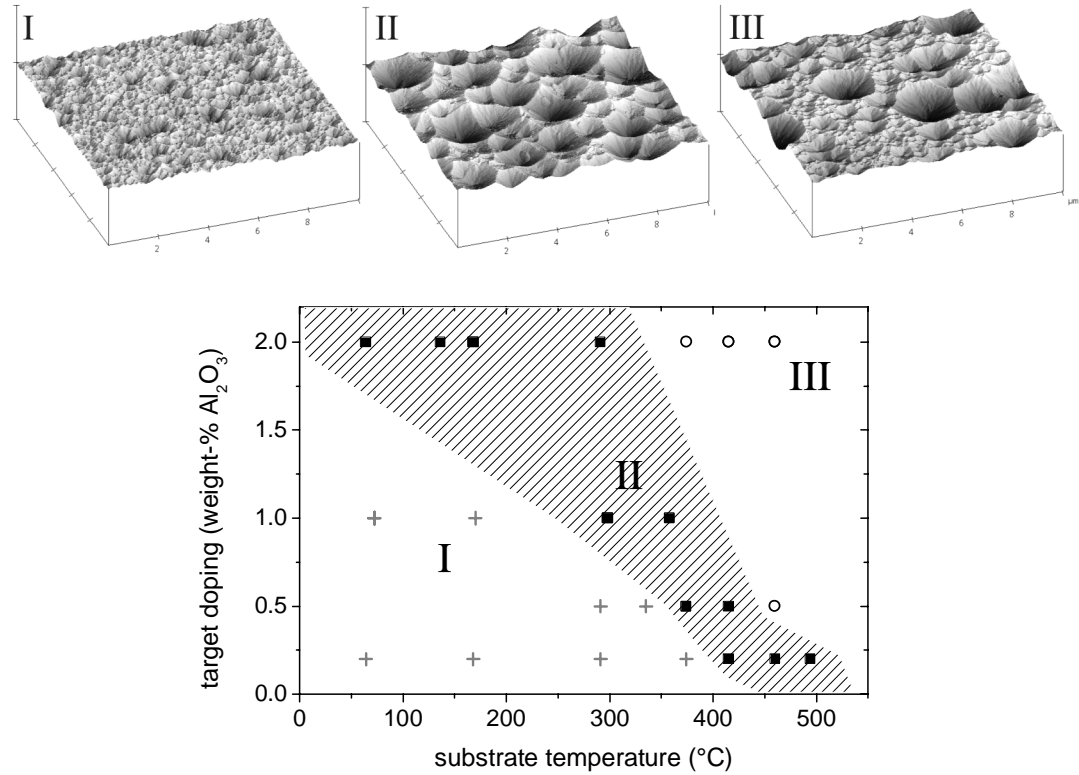


Figure 2: AFM 10x10  $\mu\text{m}^2$  measurements (top) and schematic distribution of etching behavior types in a matrix of parameters substrate temperature and TAC (crosses: type I, squares: type II, circles: type III). The parameter space where we expect to find type II films is hatched.

### 3.2 Structural ZnO:Al film properties

X-ray diffraction spectra in Bragg-Brentano geometry were measured in order to study structural properties. As it is very typical for magnetron sputtered ZnO:Al films, all films in this study exhibit a strong texture with c-axis predominantly orientated parallel to the substrate normal.

After deposition the initially smooth films have been surface-textured by wet-chemical etching in diluted hydrochloric acid (0.5 % HCl). The etching rate has been determined first and then the etching time has been adapted in a way that in average the film thickness has been typically reduced by 150 nm, leading to a final thickness of about 650 nm. Depending on the TAC and substrate temperature, three clearly different post-etching surface structures appear. The first type (denoted “I” in Fig. 2) typically comprises of a very rough surface with lateral feature sizes of about 300 nm with rather steep edges. Crater-like holes are found very rarely. For the second type (“II”) the surface topography consists of craters with diameters of about 1 to 3  $\mu\text{m}$  and depths of about 150 to 400 nm. The surface is nearly equally filled with craters of approximately same sizes. The third type (“III”) develops a rather flat surface with plenty shallow craters (depths up to about 100 nm) and few large craters: lateral diameters about 2 to 3  $\mu\text{m}$  and depths about 300 to 700 nm (limited by film thickness) in case of the big craters. The post-etching topography types I, II and III are found at different growth regimes (see Fig. 2). At low TAC and low substrate temperature only type I films are grown. The regime III with few large craters is situated at highest substrate temperatures. The transition temperature to change the regimes shifts to higher values, if TAC is reduced. Four examples for type II topographies are shown by SEM micrographs in Fig. 3. Over a broad range in TAC and substrate temperature one finds a post-etching surface topography that is equally filled with similarly sized craters. Changing the TAC has minor influence on crater-size distribution.

RMS roughness values were determined from AFM measurements and are given as function of substrate temperature in Fig. 4. Surface topographies of regime II typically have highest RMS values. In general, with surface topography changing from type I to type II the RMS values steeply increase. This transition temperature shifts to larger values with decreasing TAC. This correlates well with the predicted parameter space for regime II (see Fig. 2). A reduction in roughness is found changing from type II to type III. In case of 2.0 wt.% TAC the RMS roughness is generally rather low.

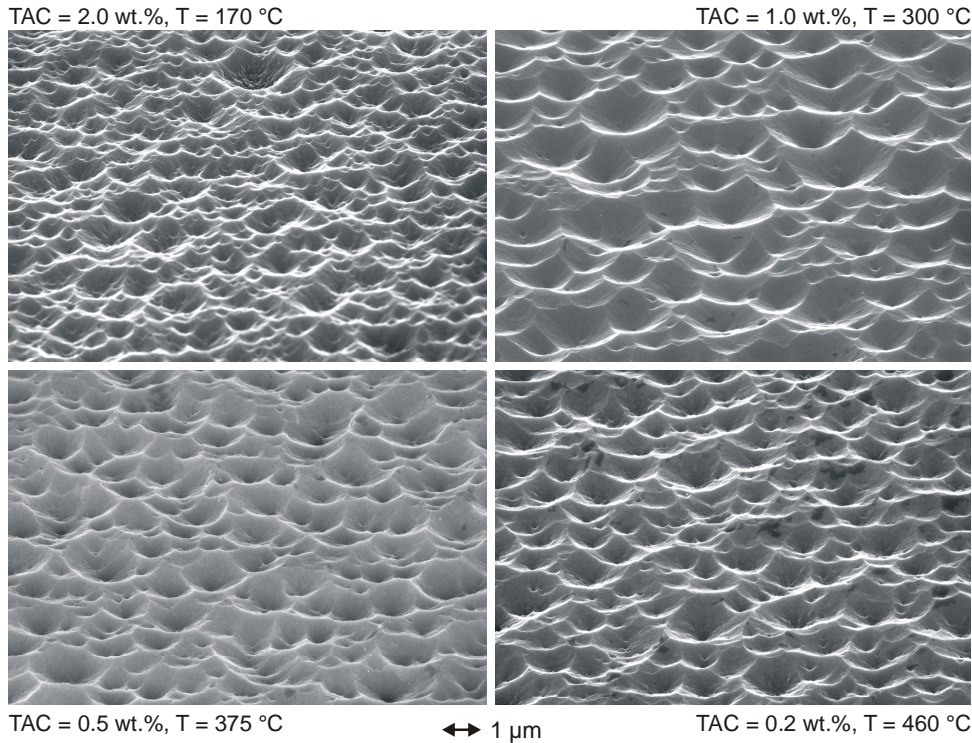


Figure 3: SEM micrographs of texture-etched ZnO:Al films of surface topography type II.

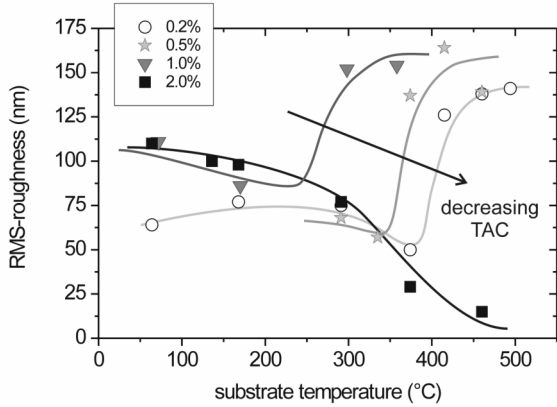


Figure 4: Root-mean-square roughness data-points calculated using the AFM measurements of texture-etched ZnO:Al films with different TAC. Guide-to-the-eye lines are drawn additionally.

Kluth et al. studied the dependence of sputter pressure and substrate temperature on the post-etching surface topography at a fixed TAC of 2 wt.% [2]. They introduced a modified Thornton model for sputter deposited ZnO:Al films in which substrate temperature and sputter pressure were the main parameters to tune the film structure and thus the post-etching surface topography. Kluth et al. have introduced three regimes: type A, B and C. Type A films were sputtered at high sputter pressures and relatively low substrate temperatures and etched homogeneously with high rate and thus did not develop crater structures. The lateral feature sizes were only in the range of 50 to 200 nm. Thus, these layers did not scatter the light effectively. Type B and C films were much denser. Type B films were deposited at rather low sputter pressure. Type C films were sputtered at very low sputter pressures or further increased substrate temperatures. Both types B and C developed craters. The type C material was very compact leading to only few craters.

Comparing this characteristics of Kluth et al. with our regimes I, II and III, one can directly correlate type B to regime II and type C to regime III. Samples resembling type A material as described by Kluth et al. were not found within the parameter space studied here. The lateral feature sizes of the type I samples are about a factor of two larger than in case of type B films. Additionally, regime I features are steeper. Thus they already scatter light significantly. Kluth et al. have predicted type A to be found at very high sputter pressures. These high pressures were not studied here. Nevertheless due to more efficient light trapping and much better electrical properties of type B (II) TCOs, they are more relevant for the usage in thin-film solar cells.

In this study we find a significant influence of TAC on film growth. In order to incorporate these findings into the modified Thornton model introduced by Kluth et al., one can rescale the substrate temperature axis with the TAC. Increasing the TAC is equivalent to decreasing the substrate temperature.

### 3.3 Solar cell results

Two attributes of the front TCOs are known to determine the cell current significantly. At first a surface topography is needed that efficiently traps the light inside the solar cell. Furthermore the amount of parasitic absorption in the front TCO should be minimized. Thus, the NIR transparency – which is mainly influenced by the free carrier absorption – has to be optimized with respect to the competing electrical and optical needs.

To study the light trapping ability in thin-film solar cells, we have applied the ZnO:Al films in  $\mu\text{c-Si:H}$  single junction cells with intrinsic  $\mu\text{c-Si:H}$  layer thickness of about 1  $\mu\text{m}$ . Fig. 5 shows a summary of cell currents in dependence of used TAC and substrate temperature. These results can partly be explained employing the RMS roughness data (see Fig. 4) and the assumption, that higher roughness implies better light trapping. Note, that this model is too simple to explain the light trapping ability correct. For a detailed discussion see [10] and [11]. In case of 2.0 wt.% TAC the topography type is changing from regime II to regime III increasing the substrate temperature from 300 to 400 °C. The rather flat areas between the big craters on the one hand reduce the roughness and on the other hand scatter the light less efficiently into the silicon. Thus, the cell current steeply drops towards a level of cells fabricated on non-textured front contacts (compare with data of Rech et al.: 15.6 mA/cm<sup>2</sup> [4]). Besides that, there is a second reducing factor for the cell current.

The depth of the big craters is only limited by the TCO thickness. Consequently, with increasing lateral crater sizes more and more substrate surface is uncovered by TCO and thus does not contribute to the generation of current. In case of 0.2, 0.5 and 1.0 wt.% TAC we have mainly studied topography types I and II. There is a rather steep increase in roughness changing the surface topography regime (Fig. 4). The cell currents observed for type II front contacts are less significantly elevated. Nevertheless highest currents are found for type II films and are found at high substrate temperatures employing a rather low TAC.

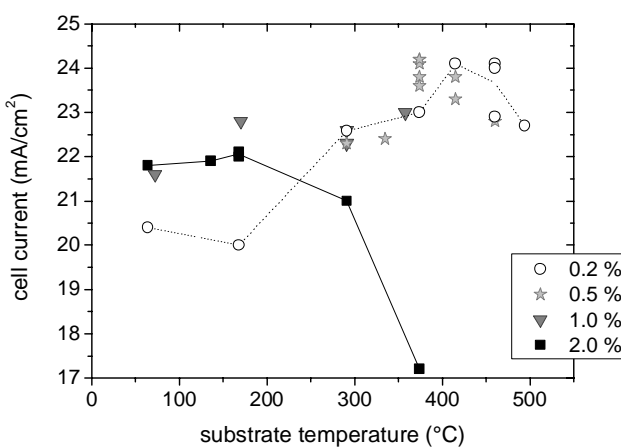


Figure 5: Current densities calculated using measured quantum efficiencies of  $\mu$ c-Si:H pin cells (i-layer thickness 1  $\mu$ m). In case of very high-ohmic front contacts the cells were measured with a negative bias of up to  $-0.5$  V in order to be able to collect all generated carriers.

Fig. 6 shows QE data and cell reflections of solar cells prepared on ZnO:Al films with different surface topography types. In case of type I topography one realizes already a certain degree of light trapping because of the roughness of these layers. Due to the poor electrical quality of the ZnO:Al film, the quantum efficiency of the corresponding cell had to be measured with negative bias applied in order to collect all generated carriers. The cell current of the cell has been  $22.1$  mA/cm $^2$ . The electrical and light trapping abilities can be improved using type II front contacts, consisting of relatively uniformly dispersed crater-like roughness. In this case the cell current has reached  $22.9$  mA/cm $^2$  due to an improved QE in the red and NIR wavelength range. The gain in efficiency is considerable due to the much better electrical properties of the ZnO:Al leading to high fill factor and open circuit voltage. A front ZnO:Al with topography of type III is remarkably less successful in trapping the light within the cell. It mainly consists of flat regions without significant light scattering, leading to low QE (cell current of only  $17.2$  mA/cm $^2$ ) and interference fringes similar to cells prepared on smooth front contacts.

Using adapted values of substrate temperature during sputtering, one finds surface topographies of type II for all the investigated TAC of 0.2, 0.5, 1.0 and 2.0 wt.%. Besides minor crater size and distribution deviations (compare Fig. 3), these front TCOs significantly differ in their parasitic absorption in the NIR spectral region simply due to their different amount of free carriers (see Fig. 1). In Fig. 7 quantum efficiencies and cell reflections of  $\mu$ c-Si:H cells using TCOs with topography type II but different TAC are compared. Increasing the NIR transparency leads to increased quantum efficiency throughout the solar spectrum. The relative gain in quantum efficiency is highest close to  $\lambda = 1$   $\mu$ m, where the absorbance of  $\mu$ c-Si:H decreases rapidly and the tail of the free carrier TCO absorption peak becomes significant. The reduced absorption in the front TCO increases the cell reflection ( $R$ ) as well. This means that the gap between quantum efficiency and  $1-R$ , which is a measure for losses, is partly closed.

To further study the relevancy of the TCO transparency on the optical cell efficiency we have deposited a series of  $\mu$ c-Si:H solar cells with varying silicon thicknesses of 0.5, 1.0 and 1.9  $\mu$ m. With increasing thickness of the intrinsic silicon layer the influence of parasitic losses in the front TCO, in the doped silicon layers and at the back reflector reduce, because the relative absorbance of the intrinsic silicon layer increases. In Fig. 8 the quantum efficiencies of the cells are shown as well as the cell reflections of the two cells with 1.9  $\mu$ m  $\mu$ c-Si:H layer. Reducing the parasitic absorption in the front TCO increases the quantum efficiency and the cell reflection, thus shortens the gap between quantum efficiency and  $1-R$ . A cell current of up to  $26.8$  mA/cm $^2$  could be reached experimentally yet. Vanecek et al.

claim a maximum cell current of  $31.5 \text{ mA/cm}^2$  (in case of a  $2 \mu\text{m}$  thick  $\mu\text{-Si:H}$  solar cell) using a Monte-Carlo simulation and nearly ideal conditions like high transparencies, Lambertian light-scattering, antireflection (AR) coating and high back contact reflectivity [12]. If we consider total reflection losses of 5 % at the glass air and TCO glass interface which can be avoided by multi-layered AR coating and the significant loss in the  $\mu\text{-p}$  layer in the blue and green part of the spectrum, the light scattering properties of the  $\text{ZnO:Al}$  films presented in our study come quite close to the limit calculated in [12].

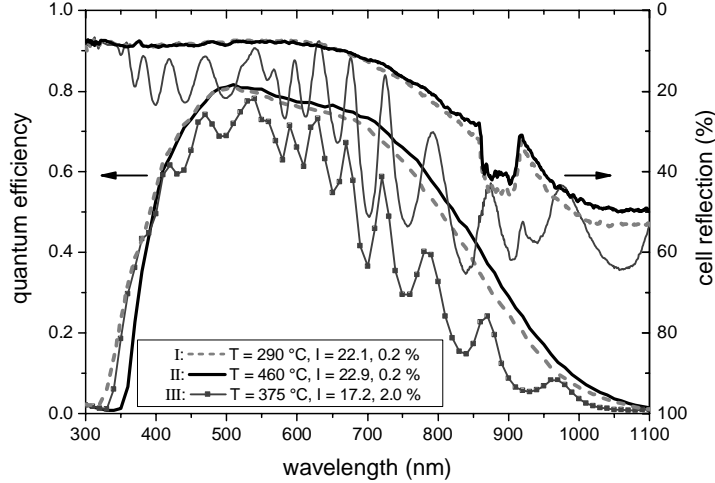


Figure 6: Quantum efficiency (left axis) and cell reflection (right axis) of a series of  $\mu\text{-Si:H}$  solar cells with intrinsic silicon layer thickness of about  $1 \mu\text{m}$ . Front TCOs of surface topography types I, II and III (see Fig. 2) have been used for TAC of 0.2 and 2.0 wt.%, respectively (see inset). Cell currents have been calculated using the solar AM1.5 spectrum (see inset, values are given in  $\text{mA/cm}^2$ ). The cell with front contact of type I has been measured with an applied bias of  $-0.5 \text{ V}$  due to poor electrical properties of the corresponding front TCO. The discontinuity in the data of the cell reflection around  $\lambda = 900 \text{ nm}$  is due to an artifact of the measurement system. Note the different direction of the right axis. In this case, the reflection curves can be interpreted as total cell absorption.

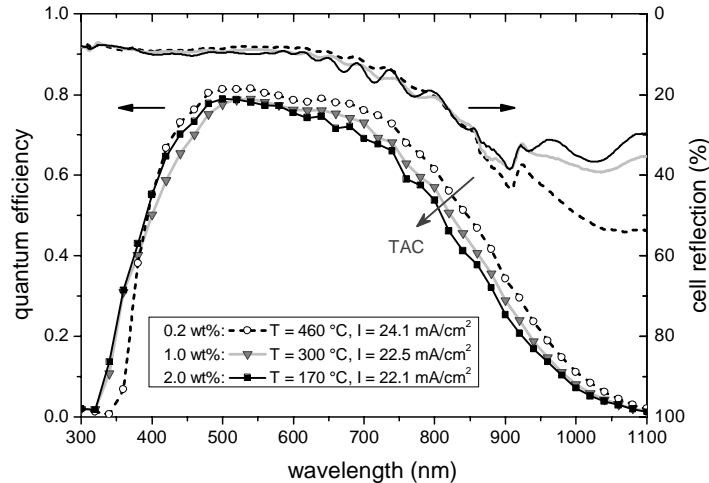


Figure 7: Quantum efficiency (left axis) and cell reflection (right axis, note different direction) of a series of  $\mu\text{-Si:H}$  solar cells. Front TCOs of surface topography type II (see Fig. 2), but different TAC have been used in order to study the influence of the parasitic TCO absorption in the NIR spectral region. The discontinuity in the data of the cell reflection around  $\lambda = 900 \text{ nm}$  is due to an artifact of the measurement system.

The quantum efficiency (**QE**) data shown in Fig. 8 has been used to estimate an effective light path enhancement factor **n**. In order to consider the different TCO absorptions **A** (see Fig. 1) during the first pass before entering the  $\mu$ -c-Si:H material **QE** is normalized to:  $\text{QE}_{\text{rescaled}} = \text{QE} / (1 - \mathbf{A})$ . The absorptions **A** has been calculated using spectrometer measurements of transmission and reflection (see Fig. 1). Using absorber layer thickness **d** and absorption coefficient  **$\alpha$**  of  $\mu$ -c-Si:H measured by photothermal deflection spectroscopy [13], one calculates the enhancement factor **n**:

$$\text{QE}_{\text{rescaled}} = 1 - \exp(-\alpha \cdot n \cdot d) \Leftrightarrow n = \frac{-\ln(1 - \text{QE}_{\text{rescaled}})}{\alpha \cdot d}.$$

This calculation of **n** assumes that every absorbed photon in the intrinsic  $\mu$ -c-Si:H material generates one electron-hole pair, that could be collected during the measurements. Thus, this simplification leads to an under-estimation of the enhancement factor, especially since it also does not consider absorption losses in the rough ZnO:Al/Ag back reflector [14].

Fig. 9 shows **n** values calculated from data in Fig. 8. For short wavelengths the value is below 1 which simply means that light of these wavelengths is absorbed in the silicon before it reaches the back reflector. At wavelengths  $\lambda > 600$  nm **n** exceeds unity, if light scattering enhances the path length geometrically and additionally, if the light is trapped between front contact and back reflector. The effective light pass enhancement factor is maximal at wavelengths  $\lambda \approx 950$  nm before it starts to decrease. The reduction in **n** in the long wavelength part of the spectrum is very likely due to gaining influence of additional parasitic absorption losses (e.g. at front and back contact). Besides this effect the surface topographies might scatter these photons less efficiently. Nevertheless, **n** values up to 16 were found. This shows that the light passes through the layers very often until finally it is absorbed or leaves the cell structure through the substrate. Thus, it is crucial to reduce parasitic absorption in photovoltaically non-active layers. The enhancement factor of the cells employing the less absorbing front TCOs are significantly larger over a broad spectral region compared with the cells using 1 wt.% TAC. Both TCOs have a post-etching topography type II and look very similar (compare Fig. 3). If we assume an equally efficient light scattering this estimation can give an idea of the importance of the NIR transparency of the front contacts. Fig. 9 shows that increasing the transparency of the front TCO results in a gain, that exceeds the gain expected from a single pass through the front TCO; since the **QE** values used for the calculation were already rescaled to compensate the effect of the first pass. Thus, the NIR absorption of the TCOs is very likely seen several times during light trapping in the cells making improvement in the transparency of the front TCO more important. Further studies untangling the effects of topography and transparency are under way.

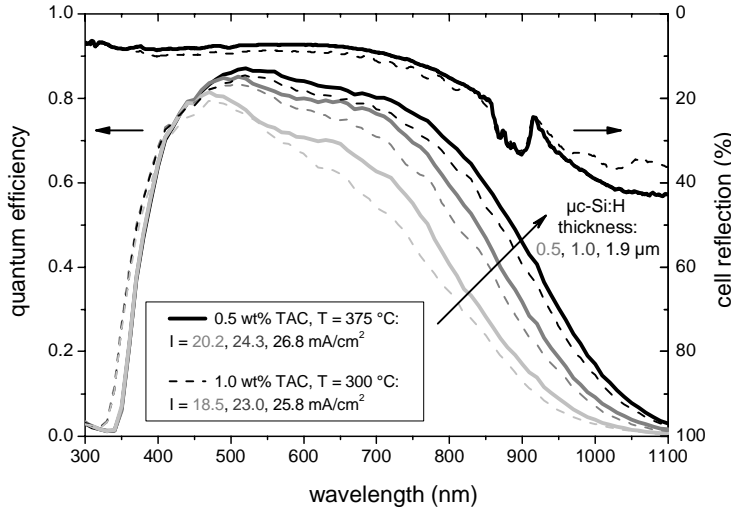


Figure 8: Quantum efficiencies (left axis) of a series of  $\mu$ -c-Si:H solar cells with varying silicon-layer thickness: 0.5, 1.0 and 1.9  $\mu$ m. On the right axis the cell reflection of the two cells with 1.9  $\mu$ m intrinsic  $\mu$ -c-Si:H is shown. The discontinuity in the data of the cell reflection around  $\lambda = 900$  nm is due to an artifact of the measurement system.

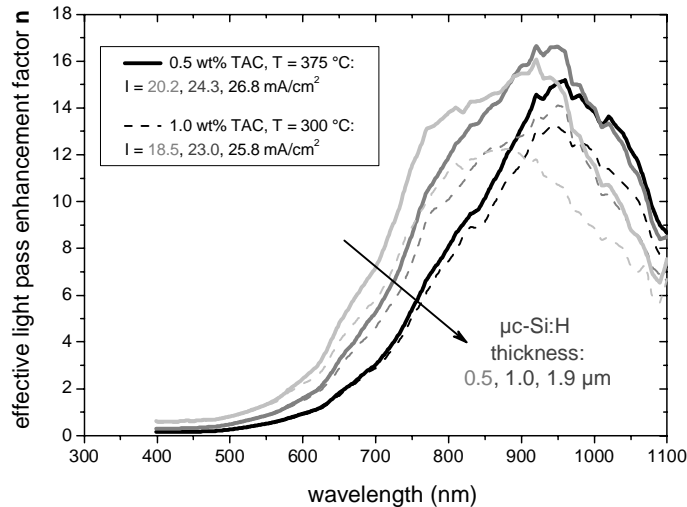


Figure 9: Effective light pass enhancement factor  $n$  calculated using quantum efficiencies of Fig. 8 and front TCO absorptions of a single pass (not shown).

## CONCLUSIONS

We have investigated the influence of the doping level of the sputter target on the post-etching surface texture of ZnO:Al films and their light trapping ability in silicon thin-film solar cells. Depending on the target aluminum concentration (TAC) and substrate temperature three different post-etching surface topography types have been found. At low TAC and low substrate temperatures during sputtering the post-etching surface topography typically comprises of a very rough surface with small lateral feature sizes (about 300 nm) and relatively steep edges. At high TAC and substrate temperatures we find a rather flat surface with plenty shallow craters (depth up to about 100 nm) and few large craters (lateral diameters up to about 3  $\mu\text{m}$  and depths limited by film thickness) after etching. Between these two parameter regimes one finds post-etching surface topographies nearly equally filled with craters of approximately same sizes (diameters about 1 to 3  $\mu\text{m}$  and depths about 150 to 400 nm).

We have investigated the performance of ZnO:Al front contacts with different amounts of parasitic absorption and topographies in thin-film silicon solar cells. The electrical properties and light trapping abilities have been improved using front contacts consisting of relatively uniformly dispersed crater-like roughness. Low TAC and relatively high substrate temperature ( $350^\circ\text{C} < T < 500^\circ\text{C}$ ) are found to be favorable for high short circuit current densities of the cells. Cell currents of up to  $26.8 \text{ mA/cm}^2$  have been realized in  $\mu\text{c-Si:H}$  single junction cell with absorber layer thickness of 1.9  $\mu\text{m}$ .

Calculations of an effective cell thickness enhancement factor of up to 16 has shown that – due to the multiple passes of the light within the cell – parasitic absorption within the ZnO:Al front contact can limit a further gain in cell current.

## ACKNOWLEDGEMENTS

The authors would like to thank G. Schöpe, A. Doumit, H. Siekmann, B. Zwaygardt, J. Kirchhoff and W. Reetz for technical assistance and H.P. Bochem for SEM measurements.

## REFERENCES

1. C. Agashe, O. Kluth, J. Hüpkens, U. Zastrow, B. Rech, "Efforts to improve carrier mobility in radio frequency sputtered aluminum doped zinc oxide films", *Journal of Applied Physics*, **95**, 1911 - 1917, 2004.
2. O. Kluth, G. Schöpe, J. Hüpkens, C. Agashe, J. Müller, B. Rech, "Modified Thornton model for magnetron sputtered zinc oxide: film structure and etching behaviour", *Thin Solid Films*, **442**, 80 - 85, 2003.

3. B. Rech, T. Roschek, T. Repmann, J. Müller, R. Schmitz, W. Appenzeller, "Microcrystalline silicon for large area thin film solar cells", *Thin Solid Films*, **427**, 157 - 165, 2003.
4. B. Rech, T. Repmann, M.N. van den Donker, M. Berginski, T. Kilper, J. Hüpkes, S. Calnan, H. Stiebig, S. Wieder, "Challenges in microcrystalline silicon based solar cell technology", *Thin Solid Films*, available online, 2005.
5. K. L. Chopra, S. Major, D. K. Pandya, "Transparent conductors – a status review", *Thin Solid Films*, **102**, 1 - 46, 1983.
6. E. Burstein, "Anomalous Optical Absorption Limit in InSb", *Physical Review*, **93**, 632 - 633, 1954.
7. T. S. Moss, "The Interpretation of the Properties of Indium Antimonide", *Proceedings of the Physical Society Section B*, **67**, 775 - 782, 1954.
8. O. Kluth, B. Rech, L. Houben, S. Wieder, G. Schöpe, C. Beneking, H. Wagner, A. Löffl, H.W. Schock, "Texture etched ZnO:Al coated glass substrates for silicon based thin film solar cells", *Thin Solid Films*, **351**, 247 - 253, 1999.
9. J. Müller, B. Rech, J. Springer, M. Vanecek, "TCO and light trapping in silicon thin film solar cells", *Solar Energy*, **77**, 917 - 930, 2004.
10. P. Lechner, R. Geyer, H. Schade, B. Rech, O. Kluth, H. Stiebig, "Optical TCO properties and quantum efficiencies in thin-film silicon solar cells", *Proceedings of the 19<sup>th</sup> European Photovoltaic Solar Energy Conference*, W. Hoffmann, J.-L. Bal, H. Ossenbrink, W. Palz, P. Helm, II, 1591 - 1594, WIP-Munich and ETA-Florence, Paris, 2004.
11. H. Stiebig, M. Schulte, C. Zahnen, C. S. Haase, B. Rech, "Light trapping in thin-film silicon solar cells by nanotextured interfaces", this proceedings, 2006.
12. M. Vanecek, J. Springer, A. Poruba, O. Kluth, T. Repmann, B. Rech, N. Wyrsch, J. Meier, A. Shah, "Light trapping and optical losses in microcrystalline Si and micromorph solar cells", *Proceedings of the 3<sup>rd</sup> World Conference on Photovoltaic Energy Conversion*, K. Kurokawa, L. L. Kazmerski, B. McNelis, M. Yamaguchi, C. Wronski, W. C. Sinke, B, 1527 - 1532, WCPEC-3 Organisation Committee, Osaka, 2003.
13. R. Carius, "Structural and optical properties of microcrystalline silicon for solar cell applications" *Photovoltaic and Photoactive Materials - Properties, Technology and Applications*, 93 - 108, Kluver Academic Publishers, Dordrecht, 2002.
14. J. Springer, A. Poruba, M. Vanecek, "Improved three-dimensional optical model for thin-film silicon solar cells", *Journal of Applied Physics*, **96**, 5329 - 5337, 2004.

\*M.Berginski@fz-juelich.de; phone +49 2461 613242 ; fax +49 2461 613735; fz-juelich.de/ipv/ipvstart\_e